Deep-Learning-Based Inverse Design of a Plasmonic Nanohole Array Metasurface for On-demand Near Field Manipulation

Jaehak Lee[1*]

[1]*Supercomputing Application Center, Korea Institute of Science and Technology Information,* [2]*University of Science and Technology, Daejeon 34141, Republic of Korea.*

** Corresponding Author: leejaehak87@gmail.com*

Abstract

Various macroscopic optical properties that are not observable in conventional homogeneous media may be realized in an optical metasurface by adjusting its sub-wavelength nanostructure. However, this requires precise and effective designing of structures. Therefore, systematic design methodologies for nanophotonic structures have garnered significant interest over the recent years. In this paper, we propose a deep-learning-based fast and efficient inverse design method for nanophotonic metasurface structures. A 10 × 10 plasmonic nanohole array structure perforated on an aluminum film was used to control both the amplitude and phase of the transmitted light with a high contrast using a small number of structural variables. To identify the structure that induces a desired field distribution, we constructed deep neural network (DNN) models that interconnected the structural variables of the plasmonic nanohole array with those of the field distributions. The DNNs were trained using data obtained via finite-difference time domain simulations. Moreover, we evaluated the performance of the proposed inverse design method for several targets, e.g., a rectangular grid with randomly determined intensities on different cells. The results confirmed an average cosine similarity of 0.86 for a field distribution at a focal length of 2,000 nm on a 4 × 4 grid with randomly determined intensities.

Keywords: Inverse design, Deep learning, Metasurface, Nanohole array, Nearfield

Introduction

Modification of the electromagnetic field of a photon via sub-wavelength metallic or dielectric nanostructures is expected to enable significant control over the properties of transmitted light. By adjusting the structural variables of the individual meta-atoms on a metasurface, the local electromagnetic properties of the transmitted or reflected light, e.g., its amplitude or phase, can be manipulated, thereby enabling full control over the entire wavefront[1-3]. This metasurface design strategy can be potentially applied in ultra-thin lenses[4], optical analog computing[5], invisibility cloaks[6], and hologram displays[7]. However, the production of high-performance metasurfaces is dependent on the development of design techniques capable of identifying optimal combinations of microscopic structures of meta-atoms that will produce the desired macroscopic characteristics of light on the entire metasurface. Consequently, systematic inverse design methodologies, including evolutionary algorithms[8], adjoint optimization techniques[9-11] and objective-first algorithms[12], have been extensively researched for metasurface designing. Most of the aforementioned design methodologies utilize iterative algorithms to identify the structures that produce recursively better results by examining structures similar to that at the previous stage. This approach produces a solution without the need to explore the entire design space. However, it is difficult to guarantee that an optimal structure identified using such a recursive method would actually be a globally optimal structure. Further, the requirement to repeat the entire iteration process for each target can increase latency, limiting its dynamic application in devices such as radars or hologram displays.

Recently, non-iterative machine-learning-based inverse design methods of several types have been extensively researched[13-16]. In these methods, the machine learning models consist of calculation procedures and inertial parameters that influence the calculation result, and the models are “trained” by fitting the inertial parameters to minimize the error between the computed results and the given dataset. As a result, the model becomes capable of identifying the solution almost immediately, unlike iterative algorithms. Further, such models can predict the solutions even for points corresponding to absent data, thus requiring significantly smaller number of trials compared to simple data-driven methods that are not based on machine learning models, e.g., Monte–Carlo methods. Among the multiple machine learning models, deep neural network (DNN) models have garnered the majority of interest for interpolating physics models and developing inverse design algorithms[17-19]. By adjusting several hyper-parameters, such as the number of layers or the number of neurons per layer, DNN models can be flexibly optimized for each problem. Several studies have been published on the inverse design of metasurfaces based on DNN models[20-24]. However, in most of the recent reports, the role of the DNN model is limited to the

design of individual meta-atoms corresponding to local electromagnetic responses. Thus, additional procedures are still required to identify the total combination of the local electromagnetic responses for a target macroscopic field distribution. In addition, incorporating the interactions between meta-atoms in this process is difficult; thus, the range of possible structures remains limited to those with weak interactions between meta-atoms.

In this paper, we propose a deep-learning-based inverse design method capable of designing the entire metasurface structure, including the structural variables of each meta-atom simultaneously. The method utilizes a "designer DNN" that lists the structural variables for a given target field distribution and a "simulator DNN" that produces the field distribution corresponding to a given structure. Using the designer DNN, the overall structure of the metasurface can be directly determined without implementing any iterative process. Subsequently, the resultant field distribution obtained from the designed structure can be immediately predicted and verified using the simulator DNN. Here, we demonstrate the application of the proposed method in designing a metasurface consisting of 10 × 10 arrays of sub-wavelength holes, with different diameters, perforated on a thin aluminum film. Owing to plasmonic resonances in individual holes or between the holes, the nanohole structures perforated on metallic films are known to influence the light, passing through the structure, with a very high contrast[25-33]. By manipulating only the diameters of the holes, local optical properties, such as the amplitude or phase, of the light transmitted through each hole can be modulated within a broad range (See Supplemental Material 1), and then integrated to form diverse near field distributions using the proposed inverse design method. Experimental results confirmed that when light of 650-nm wavelength was transmitted through the metasurface containing nanohole arrays, the two-dimensional nearfield distributions over an area of 5.4 μm × 5.4 μm at a distance of 500–5,000 nm from the surface could be controlled by adjusting the period of the array, diameters of the holes, and source power. The proposed inverse design method has potential application in fields that require on-demand control of near field distributions, such as lithography[34-36], photovoltaics[37] and bio-detection[38].

Results

Figure 1a depicts a schematic of the metasurface structure, with nanohole arrays, and transmission of incident light. In every simulation reported in this study, the metasurface was assumed to have been fabricated on a glass substrate, and the incident light was assumed to be a normally incident plane wave polarized along the horizontal axis of the nanohole array, with the source on the side of the substrate. Based on the analysis of a single-hole

structure (See Supplemental Material 1), a 10 × 10 array of holes (diameter of each hole: 100–325 nm) perforated on an aluminum layer on a glass substrate, with period in the range of 375–550 nm, was considered as the metasurface structure. The thickness of the aluminum layer was considered to be 150 nm, which is sufficient to prevent the penetration of incident light without passing through the holes while providing sufficient phase shift to the light transmitted through the holes. A two-dimensional distribution of electric-field energy density ($\varepsilon|E|^2$) over an area of 5.4 μm × 5.4 μm at varying distances (z) from and parallel to the metasurface was considered as field distribution to be controlled. The electric field distribution corresponding to each metasurface structure was calculated via finite-difference time domain (FDTD) simulations. A full-vectorial complex near field distribution (i.e., near field amplitudes) was obtained via Fourier transformation of the time-record of the electric field at each point on a 5.4 μm × 5.4 μm area at a distance of 325 nm from the metasurface, considering a gaussian plane wave, corresponding to a 650-nm incident light, normally incident on the surface from the substrate side. Based in this distribution, the electric-field energy density distributions at arbitrary distances (z) (i.e., Fresnel field intensities) can be obtained using the Fresnel integral method. We ignored the area outside the designated 5.4 μm × 5.4 μm region for the Fresnel integral as the aluminum layer was assumed to be sufficiently thick to prevent direct penetration of light. Several simulations were performed on the structures randomly generated from the structural variables, following the uniform distribution within the aforementioned range, to obtain the structure–field data pairs for training the simulator and designer DNNs.

Figure 1b depicts a schematic of the internal structure, input variables, and output variables of the two DNN models used in the proposed inverse design method. The simulator DNN receives the structural variables (array period and diameters of each hole) as the input variables and returns the near field amplitudes as the output variables. Subsequently, the Fresnel field intensities at arbitrary distances (z) are obtained using the Fresnel integral method, based on the output of the simulator DNN. As illustrated in Figure 1b, the structure of the simulator DNN consisted of two sequential layers with 8,000 neurons in each layer. The adjacent layers were fully connected by a rectified linear unit (ReLU) activation function. The structure of the designer DNN consisted of five sequential layers with 8,000 neurons in each layer, in which the adjacent layers were fully connected by a ReLU activation function. The designer DNN receives the Fresnel field intensities over the 5.4 μm × 5.4 μm area at a resolution of 108 × 108 corresponding to a specific distance (z) as the input variable and returns the array period, diameters of the holes on the array, and source power that generates the given field distribution as the output variables. The source power values were randomly generated to ensure that the

logarithms followed a normal distribution and were multiplied to the target Fresnel field intensities before each iteration of the fitting process. This process enabled the inverse design method to reproduce similar field distributions with varying absolute amplitudes by adjusting the source power, making the method capable of addressing more diverse field distributions. We used the results obtained from 12,924 FDTD simulations to develop the training dataset that was used to train both the simulator and designer DNN models, and used 1,292 results to generate the test dataset that was used to validate the two DNN models. During the training process, the weight parameters of the neurons were optimized using the Adam algorithm to minimize the mean squared errors between the output training data and the returned values corresponding to the input training data.

Figures 2a–f depict the nanohole array structures, near field amplitudes predicted using the simulator DNN model, and near field amplitudes predicted using the FDTD simulations. As illustrated in Figures 2a–b, the horizontal cross-sections of the metasurfaces were of irregular shapes because of the randomly generated array period and diameters. The near field amplitudes of the light transmitted through these metasurfaces were obtained using the simulator DNN, as depicted in Figures 2c and 2e. A comparison of the predicted fields with the simulated fields (Figures 2d and 2f, respectively) revealed that, even in the case with the maximum MAE out of the 1,292 test data cases, a good agreement is observed between the two. Thus, it was proved that the simulator DNN can be used to verify the accurate generation of the field distribution corresponding to various structures designed using the designer DNN, without performing complete FDTD simulations. Figure 2g depicts the MAEs of the near field amplitudes predicted using the simulator DNNs that were trained using varying quantities of data. When the number of training data points was considered to be small, the MAE of the training data (i.e., training error) was significantly low, while that of the test data (i.e., test error) was high. As the number of training data was increased, the training error increased, whereas the test error decreased, indicating that the two values approached each other. This can be attributed to the overfitting of the model when the number of training data is insufficient compared to the degrees of freedom of the model. Therefore, in order to construct a simulator DNN that produces consistently accurate predictions on both the training and test data, a large number of training data along with a high degree of freedom of the model are required simultaneously.

As the performance of an inverse design method should be evaluated in terms of the accuracy of reproduction of the target distributions, we analyzed the differences between the target Fresnel field intensities and the corresponding fields produced by the predicted structures (i.e., field MAE) as well as the differences between the structures that originally produced the target fields and the corresponding predicted structures (i.e., structure

MAE). Figures 3a–b summarize the results obtained by training the designer DNN corresponding to target Fresnel field intensities at z = 2,000 nm with various quantities of training data. As the number of training data was increased, both the field and structure MAEs of the test data were observed to decrease. During this analysis, we used the simulator DNN instead of full FDTD simulations to obtain the field distributions produced from the predicted structures and to calculate the field MAE. Figures 3c–e depict some representative results for the cases where the field MAEs were equal to the median, field MAEs equal to the 95 % percentile, and field MAEs were maximum, respectively. For each given target field, the designer DNN returned the inverse-designed structures. Then, the field distributions of the designed structures were predicted using the simulator DNN and Fresnel integrals. In the cases where the field MAEs were equal to the median (Figure 3c) and 95 % percentile (Figure 3d), both the predicted structures and fields exhibited good agreement with the original structures and target fields. In the case with the maximum MAE (Figure 3e), although the structure was slightly different from the original structure, the resultant field distribution exhibited reasonable agreement with the target distribution. Moreover, the field distributions obtained using the simulator DNN were consistent with the results obtained via full FDTD simulations.

However, the aforementioned favorable results on the test dataset are alone not sufficient proof of the viability of the proposed inverse design method, because the test dataset is not representative of the overall design space. In fact, although any simulated field distribution in the test dataset has a corresponding structure that can reproduce itself, this is not a guaranteed condition for arbitrary field distributions. Therefore, further experiments on the arbitrary target field distributions are required to evaluate the accuracy of reproduction of the diverse field distributions properly. Accordingly, we first tested the performance of the designer DNN corresponding to point-like target field distributions at varying positions and with varying numbers of points, as illustrated in Figure 4. In the target distributions, each point target was represented by a circle with a diameter of 325 nm, which is half of the wavelength. The amplitude of each point target was selected by considering an appropriate operation range. For single-point targets, the distributions corresponding to holes of varying diameters yielded concentric circles that resembled an interference pattern around the target point, and the resulting field distribution was also well focused at the center of the concentric circles, as depicted in Figures 4a–f. As illustrated in Figures 4a–c, the diameters of the concentric circles increased with the increasing distance (z). Further, as shown in Figures 4c–f, when the target point was displaced horizontally, the concentric pattern followed the movement, ensuring the successful reproduction of the resultant field distributions at the edges of the target region.

Notably, the formation and subsequent movement of the concentric pattern appeared to cause constructive interference at a given point, even though the designer DNN model was not trained about the interference principle. In addition, when two points were simultaneously given at the target, a hole array structure was formed, with the concentric circles corresponding to the two points overlapping each other. Moreover, when the distance between the two points was increased, the centers of the concentric circles exhibited a similar movement, as depicted in Figures 4g–h. Thus, the two points were observed to be well-expressed on the reproduced field distributions.

To investigate the effect of the distance between the target region and the metasurface (z), we considered chessboard-like target field distributions (Figure 5a–c) and compared the results obtained using the designer models trained corresponding to varying distances, as depicted in Figures 5d–i. The dependence of the structures on the distance between the target region and the metasurface revealed that the shape of the hole diameter distribution approached the target field distribution as the distance was decreased. In contrast, as the distance was increased, the boundaries of the structural distribution became wider and more ambiguous, similar to a diffraction interference pattern. Moreover, the designed structures corresponding to too small or too large distances did not accurately reproduce the target patterns. The target field distribution was reproduced with the highest accuracy when the distance was in the range of 1,500–2,000 nm. The results indicated that the distance between the target region and the metasurface should be sufficiently large to ensure that the light transmitted through the holes cooperatively interferes to enable an effective control over the field distribution. Simultaneously, the distance should be sufficiently small to ensure a sensitive dependence of the optical path length on the horizontal displacements in position, which affects the spatial resolution in the horizontal direction.

Finally, to consider a frame for the definition of an arbitrary target field distribution, we divided the target area using a rectangular grid and randomly assigned field intensities to each cell of the grid. Figures 6a–c depict the obtained results corresponding to the cases with median and maximum field MAEs among the 300 random target distributions considered for 2 × 2, 3 × 3, and 4 × 4 grids, respectively. The field intensity at each grid region was randomly generated from a uniform distribution in the range optimized for the best reproduction performance. The distance between the region and the metasurface was set to 2,000 nm. The results indicated that, in the cases of median and maximum field MAEs, the resulting field distribution corresponded closely to the target field distribution, as illustrated in Figures 6a–c. Quantitatively, the average cosine similarities were 0.87, 0.83, and 0.86 corresponding to the 2 × 2, 3 × 3, and 4 × 4 grids, respectively. This is expected to serve as a reference for future studies.

Conclusions

In this study, a deep-learning-based inverse design method for metasurfaces was proposed to manipulate the field distributions of the transmitted light. To increase the diversity of the available field distributions efficiently using a small number of structural variables, we considered a metasurface structure consisting of an array of plasmonic nanoholes capable of profoundly influencing the amplitude and phase of the transmitted light. By constructing a designer DNN model that directly interconnects the field distributions with the structural variables of the metasurfaces, an optimal structure capable of reproducing a target field distribution was directly obtained, without iterative trial and error processes. In addition, using the simulator DNN models, the field distributions of the inverse-designed structures could be immediately verified without performing time-consuming simulations. Consequently, we verified that the designer DNN models trained using sufficient quantities of data can be used to identify the structures that accurately reproduce several types of target field distributions, e.g., single point, multiple points, chessboard-like patterns, and randomly generated field distributions on 2 × 2, 3 × 3, and 4 × 4 grids. The proposed inverse design method, combined with active metasurfaces[39], can be applied in dynamic processes that require on-demand electromagnetic wave manipulation, such as beam steering[40,41] and optical manipulation[42].

Acknowledgements

This work was supported by Basic Science Research Program through the National Research Foundation of Korea (NRF) funded by the Ministry of Education (2019R1A6A3A01094872)

Additional information

Supplemental Material accompanies this paper at online

Figures

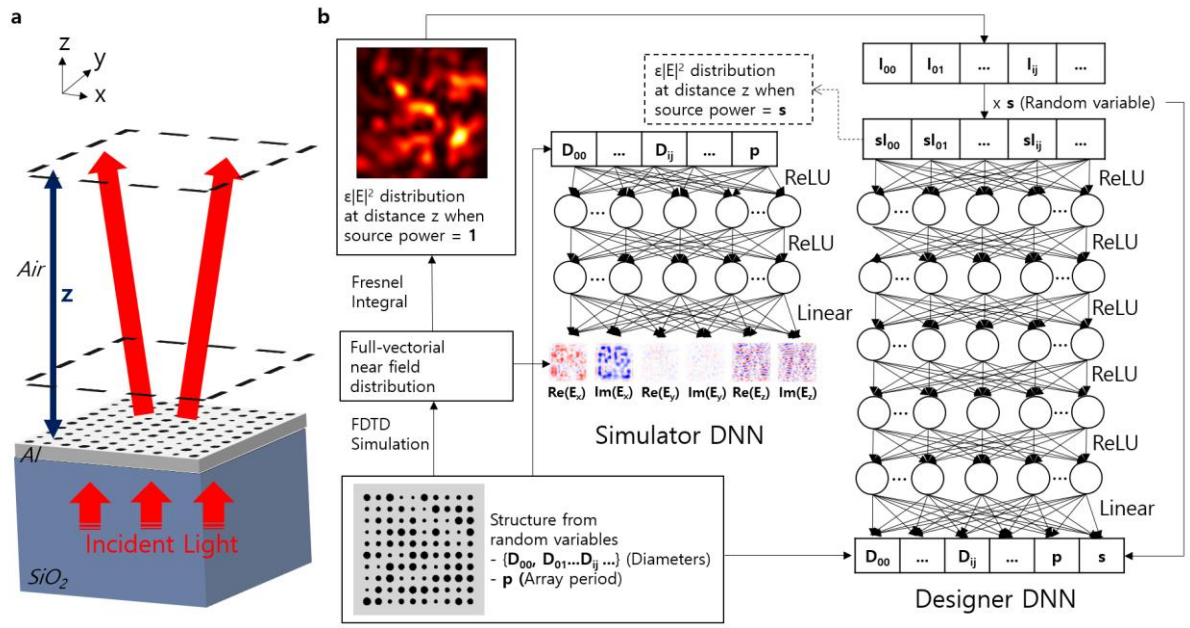

Figure 1 | Overview. (a) Conceptual diagram of the structure and operation of the plasmonic nanohole array metasurface. The red arrows indicate the loci of propagation of incident light. (b) Schematic diagram of the simulator DNN model, the designer DNN model, and visualization of the definitions of the input and output features.

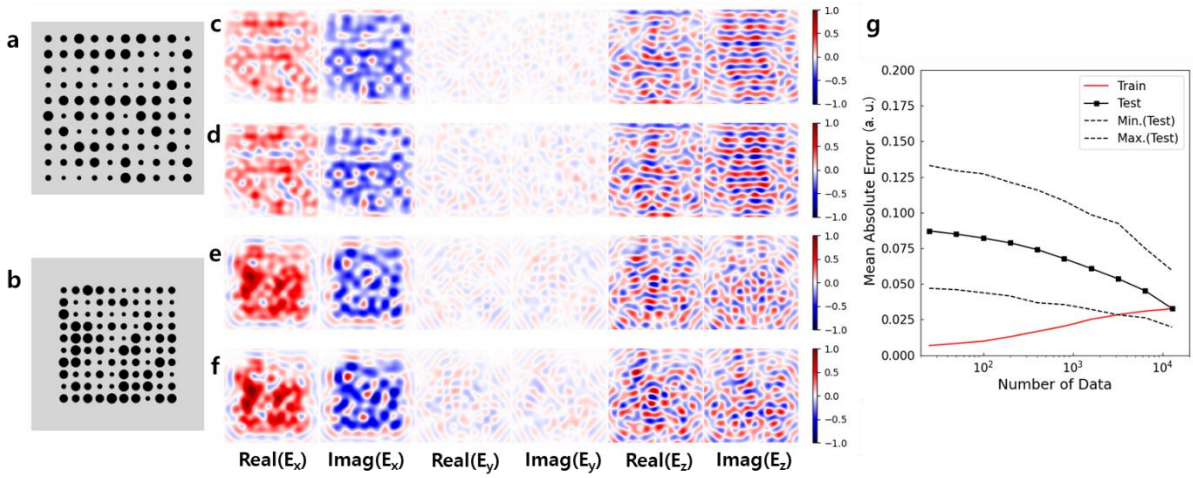

Figure 2 | Simulator DNN. (a–b) Cross-sectional views of the nanohole array structures. (c-f) Near field amplitudes predicted using (c, e) the simulator DNN and (d, f) FDTD simulation. The complex vector components are specified below each column in the figure. (a, c, d) Median MAE case and (b, e, f) Maximum MAE among the structures in the test dataset. (g) MAEs of the outputs of the simulator DNNs trained using various quantities of training data, which were averaged over the training dataset (red solid line), averaged over the test dataset (black solid line), and the smallest and the largest MAEs corresponding to the test dataset (black dashed lines).

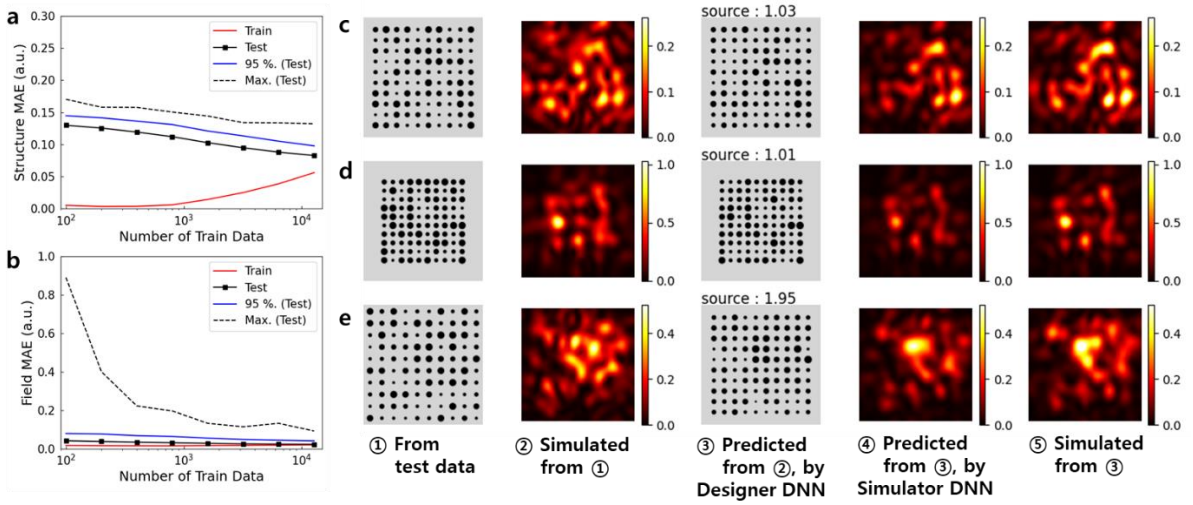

Figure 3 | Designer DNN. (a) Structure MAEs and (b) field MAEs, which were averaged over the training dataset (red solid lines), averaged over the test dataset (black solid lines with squares), the 95 % percentile MAEs in the test dataset (blue solid lines), and the maximum MAE in the test dataset (black dashed lines). (c–e) Original structures, simulated fields corresponding to the original structures, inverse designed structures with source powers that produce the simulated fields, and predicted and simulated fields corresponding to the inverse designed structures in the cases in which the (c) field MAEs are equal to the median, (d) field MAEs are equal to the 95 % percentile, and (e) field MAEs are maximum.

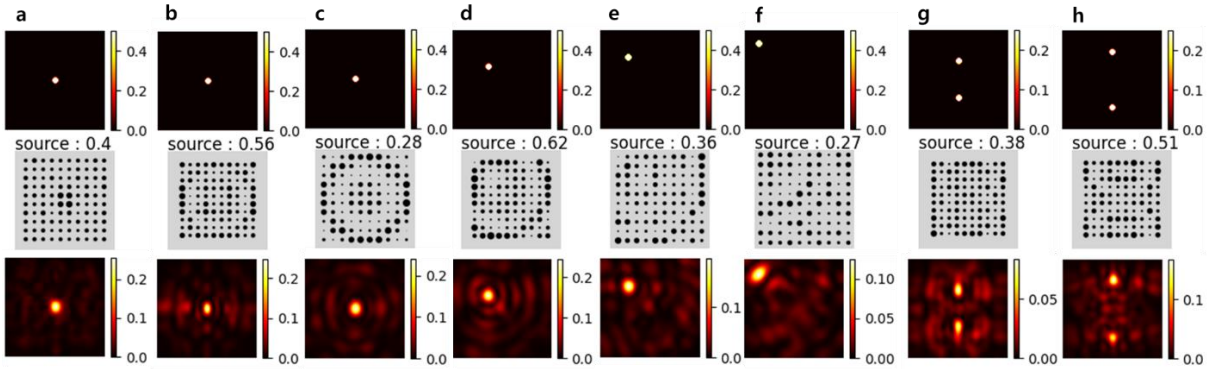

Figure 4 | Inverse design for point targets (a–h) Target field distributions, inverse-designed structures with source powers corresponding to the target field distributions, and simulated field distributions corresponding to the designed structures, (a–f) for single point targets where (a) z =1,000 nm, (b) z = 2,000 nm, (c–f) z = 4,000 nm corresponding to varying horizontal positions, (g–h) for double point targets where z = 2,000 nm corresponding to varying distances between the points.

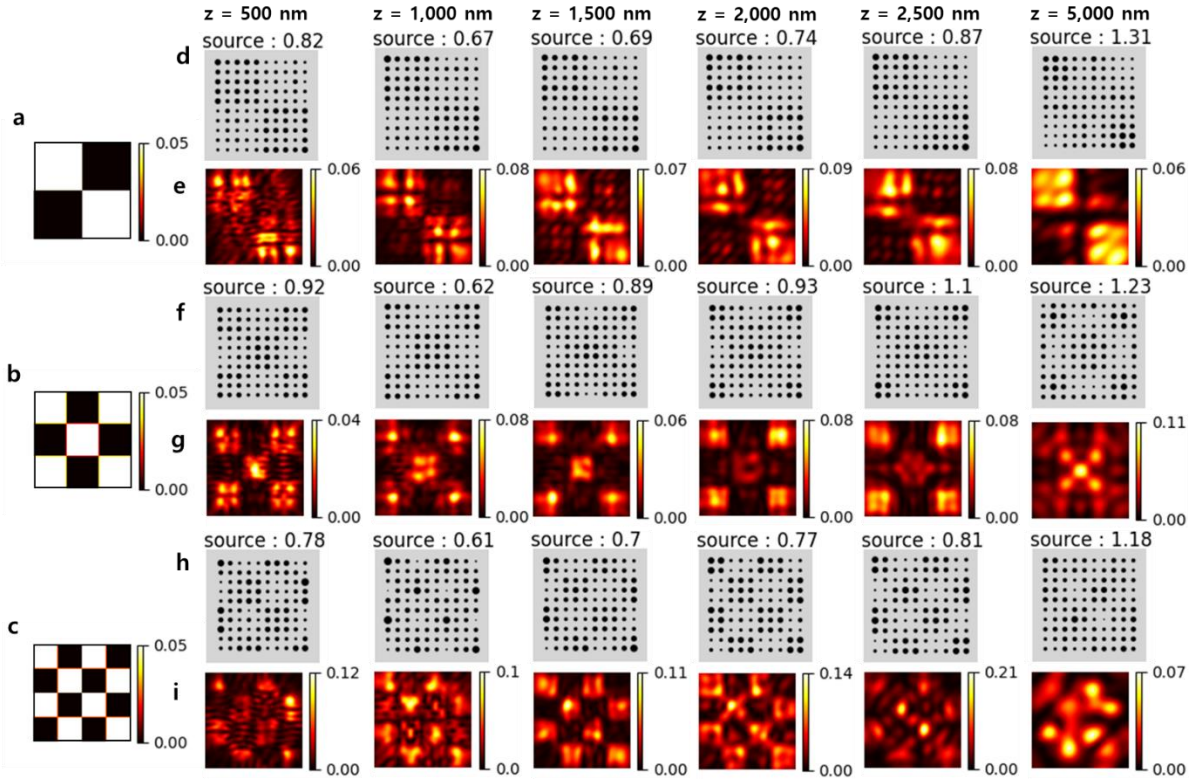

Figure 5 | Effect of distance from the metasurface. (a–c) Target field distributions. (d, f, h) Inverse-designed structures with source powers and (e, g, i) simulated field distributions corresponding to the designed structures, (d–e) corresponding to the target field distribution of (a), (f–g) corresponding to the target field distribution of (b) and (h–i) corresponding to the target field distribution of (c), respectively, at various distances from the metasurface.

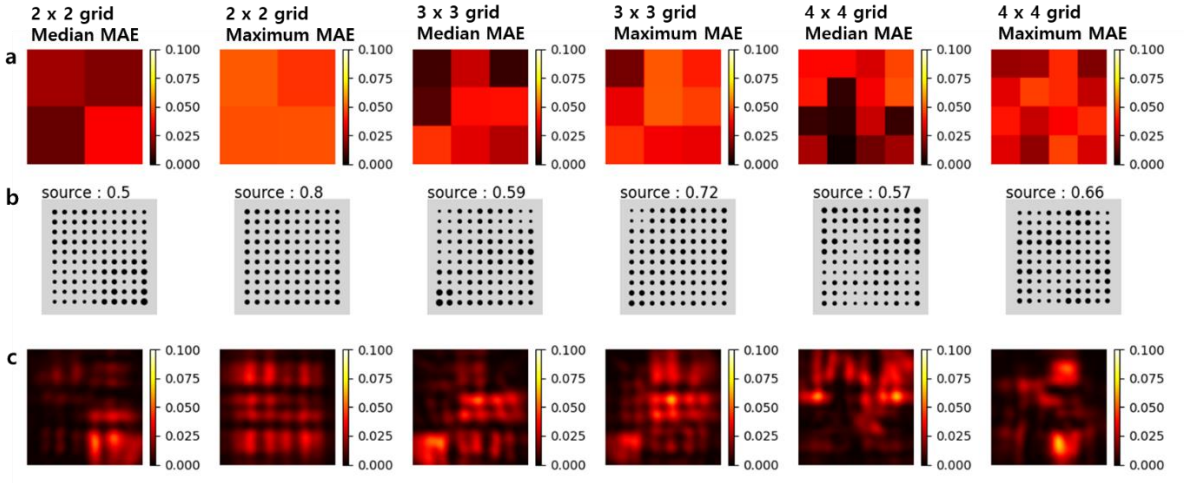

Figure 6 | Inverse design for random target field distributions. (a) Target field distributions, (b) inverse-designed structures with source powers corresponding to the target fields, and (c) simulated field distributions corresponding to the inverse-designed structures corresponding to the median and the maximum field MAE cases for 2 × 2, 3 × 3, and 4 × 4 grids.

References

1 Yu N, Genevet P, Kats MA, Aieta F, Tetienne J-P *et al.* Light Propagation with Phase Discontinuities: Generalized Laws of Reflection and Refraction. *Science* 2011; **334**: 333-337.

2 Yu N, Capasso F. Flat optics with designer metasurfaces. *Nature Materials* 2014; **13**: 139-150.

3 Meinzer N, Barnes WL, Hooper IR. Plasmonic meta-atoms and metasurfaces. *Nature Photonics* 2014; **8**: 889-898.

4 Ni X, Ishii S, Kildishev AV, Shalaev VM. Ultra-thin, planar, Babinet-inverted plasmonic metalenses. *Light-Science & Applications* 2013; **2**: e72.

5 Silva A, Monticone F, Castaldi G, Galdi V, Alù A *et al.* Performing Mathematical Operations with Metamaterials. *Science* 2014; **343**: 160-163.

6 Ni X, Wong ZJ, Mrejen M, Wang Y, Zhang X. An ultrathin invisibility skin cloak for visible light. *Science* 2015; **349**: 1310-1314.

7 Huang L, Chen X, Mu¨Hlenbernd H, Zhang H, Chen S *et al.* Three-dimensional optical holography using a plasmonic metasurface. *Nature Communications* 2013; **4**: 2808.

8 Jafar-Zanjani S, Inampudi S, Mosallaei H. Adaptive Genetic Algorithm for Optical Metasurfaces Design. *Scientific Reports* 2018; **8**.

9 Dühring MB, Sigmund O. Optimization of extraordinary optical absorption in plasmonic and dielectric structures. *Journal of the Optical Society of America B-Optical Physics* 2013; **30**: 1154-1160.

10 Lalau-Keraly CM, Bhargava S, Miller OD, Yablonovitch E. Adjoint shape optimization applied to electromagnetic design. *Optics Express* 2013; **21**: 21693-21701.

11 Mansouree M, Kwon H, Arbabi E, Mcclung A, Faraon A *et al.* Multifunctional 2.5D metastructures enabled by adjoint optimization. *Optica* 2020; **7**: 77-84.

12 Callewaert F, Velev V, Kumar P, Sahakian AV, Aydin K. Inverse-Designed Broadband All-Dielectric Electromagnetic Metadevices. *Scientific Reports* 2018; **8**: 1358.

13 Elsawy MMR, Lanteri S, Duvigneau R, Brière G, Mohamed MS *et al.* Global optimization of metasurface designs using statistical learning methods. *Scientific Reports* 2019; **9**: 17918.

14 Melati D, Grinberg Y, Dezfouli MK, Janz S, Cheben P *et al.* Mapping the global design space of nanophotonic components using machine learning pattern recognition. *Nature Communications* 2019; **10**: 4775.

15 Qin F, Zhang D, Liu Z, Zhang Q, Xiao J. Designing metal-dielectric nanoantenna for unidirectional scattering via Bayesian optimization. *Optics Express* 2019; **27**: 31075-31086.

16 Sajedian I, Badloe T, Rho J. Optimization of colour generation from dielectric nanostructures using reinforcement learning. *Optics Express* 2019; **27**: 5874-5883.

17 Liu D, Tan Y, Khoram E, Yu Z. Training Deep Neural Networks for the Inverse Design of Nanophotonic Structures. *Acs Photonics* 2018; **5**: 1365-1369.

18 Tahersima MH, Kojima K, Koike-Akino T, Jha D, Wang B *et al.* Deep Neural Network Inverse Design of Integrated Photonic Power Splitters. *Scientific Reports* 2019; **9**: 1368.

19 Wiecha PR, Muskens OL. Deep Learning Meets Nanophotonics: A Generalized Accurate

Predictor for Near Fields and Far Fields of Arbitrary 3D Nanostructures. *Nano Lett.* 2020; **20**: 329-338.

20 Liu Z, Zhu D, Rodrigues SP, Lee K-T, Cai W. Generative Model for the Inverse Design of Metasurfaces. *Nano Lett.* 2018; **18**: 6570-6576.

21 Malkiel I, Mrejen M, Nagler A, Arieli U, Liorwolf *et al.* Plasmonic nanostructure design and characterization via Deep Learning. *Light-Science & Applications* 2018; **7**: 60.

22 Nadell CC, Huang B, Malof JM, Padilla AWJ. Deep learning for accelerated all-dielectric metasurface design. *Optics Express* 2019; **27**: 27523-27535.

23 An S, Zheng B, Shalaginov MY, Tang H, Li H *et al.* Deep learning modeling approach for metasurfaces with high degrees of freedom. *Opt Express* 2020; **28**: 31932-31942.

24 Singh R, Agarwal A, Anthony BW. Design of optical meta-structures with applications to beam engineering using deep learning. *Sci Rep* 2020; **10**: 19923.

25 Martín-Moreno L, García-Vidal FJ, Lezec HJ, Pellerin KM, Thio T *et al.* Theory of extraordinary optical transmission through subwavelength hole arrays. *Physical Review Letters* 2001; **86**: 1114-1117.

26 Genet C, Ebbesen TW. Light in tiny holes. *Nature* 2007; **445**: 39-46.

27 Matsui T, Agrawal A, Nahata A, Vardeny ZV. Transmission resonances through aperiodic arrays of subwavelength apertures. *Nature* 2007; **446**: 517-521.

28 Garcia-Vidal FJ, Martin-Moreno L, Ebbesen TW, Kuipers L. Light passing through subwavelength apertures. *Reviews of Modern Physics* 2010; **82**: 729-787.

29 Kang M, Feng T, Wang H-T, Li J. Wave front engineering from an array of thin aperture antennas. *Optics Express* 2012; **20**: 15882-15890.

30 Vynck K, Burresi M, Riboli F, Wiersma DS. Photon management in two-dimensional disordered media. *Nat Mater* 2012; **11**: 1017-1022.

31 Yokogawa S, Burgos SP, Atwater HA. Plasmonic color filters for CMOS image sensor applications. *Nano Lett* 2012; **12**: 4349-4354.

32 Lee J, Sung S, Choi J-H, Eom SC, Mortensen NA *et al.* Ultra sub-wavelength surface plasmon confinement using air-gap, sub-wavelength ring resonator arrays. *Sci Rep* 2016; **6**: 22305.

33 Lee J, Yang S, Lee J, Choi J-H, Lee Y-H *et al.* Extraordinary optical transmission and second harmonic generation in sub–10-nm plasmonic coaxial aperture. *Nanophotonics* 2020; **9**: 3295-3302.

34 Lama EY, Wong AKK. Computation lithography: virtual reality and virtual virtuality. *Optics Express* 2009; **17**: 12259-12268.

35 Shen Y, Wong N, Lam EY. Level-set-based inverse lithography for photomask synthesis. *Optics Express* 2009; **17**: 23690-23701.

36 Shen Y, Jia N, Wong N, Lam EY. Robust level-set-based inverse lithography. *Optics Express* 2011; **19**: 5511-5521.

37 Xiao TP, Cifci OS, Bhargava S, Chen H, Gissibl T *et al.* Diffractive Spectral-Splitting Optical Element Designed by Adjoint-Based Electromagnetic Optimization and Fabricated by

Femtosecond 3D Direct Laser Writing. *Acs Photonics* 2016; **3**: 886-894.

38 Yesilkoy F, Cevher V, Kivshar Y, Arvelo ER, Jahani Y *et al.* Ultrasensitive hyperspectral imaging and biodetection enabled by dielectric metasurfaces. *Nature Photonics* 2019; **13**: 390-396.

39 Shaltout AM, Shalaev VM, Brongersma ML. Spatiotemporal light control with active metasurfaces. *Science* 2019; **364**: 648.

40 Battal E, Okyay AK. Metal-dielectric-metal plasmonic resonators for active beam steering in the infrared. *OPTICS LETTERS* 2013: 983-985.

41 Ito H, Kusunoki Y, Maeda J, Akiyama D, Kodama N *et al.* Wide beam steering by slow-light waveguide gratings and a prism lens. *Optica* 2020; **7**: 47-52.

42 Dholakia K, Čižmár T. Shaping the future of manipulation. *Nature Photonics* 2011; **5**: 335-342.

Supplemental Material

Deep-Learning-Based Inverse Design of a Plasmonic Nanohole Array Metasurface for On-demand Near Field Manipulation

Jaehak Lee[1*]

[1]Supercomputing Application Center, Korea Institute of Science and Technology Information, [2]University of Science and Technology, Daejeon 34141, Republic of Korea.

** Corresponding Author: leejaehak87@gmail.com*

1. Characterization of the optical transmission through a single hole structure

Figure S1 summarizes characterization of the optical transmission through a single hole structure which is a unit meta-atom of the overall meta-surface. The aluminum layer is on the glass substrate, and a plane-wave polarized along the x direction is normally incident from the substrate side. Figure S1a-c summarizes phase and amplitude (E_x) of the transmitted 650 nm light with varying hole-diameters and aluminum thickness. As shown in Figure S2b, the contrast of amplitude depending on the diameter is very high, and the contrast increases as the aluminum layer thickness increases. Also, as shown in Figure S1c, the degree of phase shift according to diameter also increases as the aluminum thickness increases. In example, when the aluminum thickness is 150 nm, the phase difference is 2.4 radian when the diameter is changed from 100 nm to 325 nm.

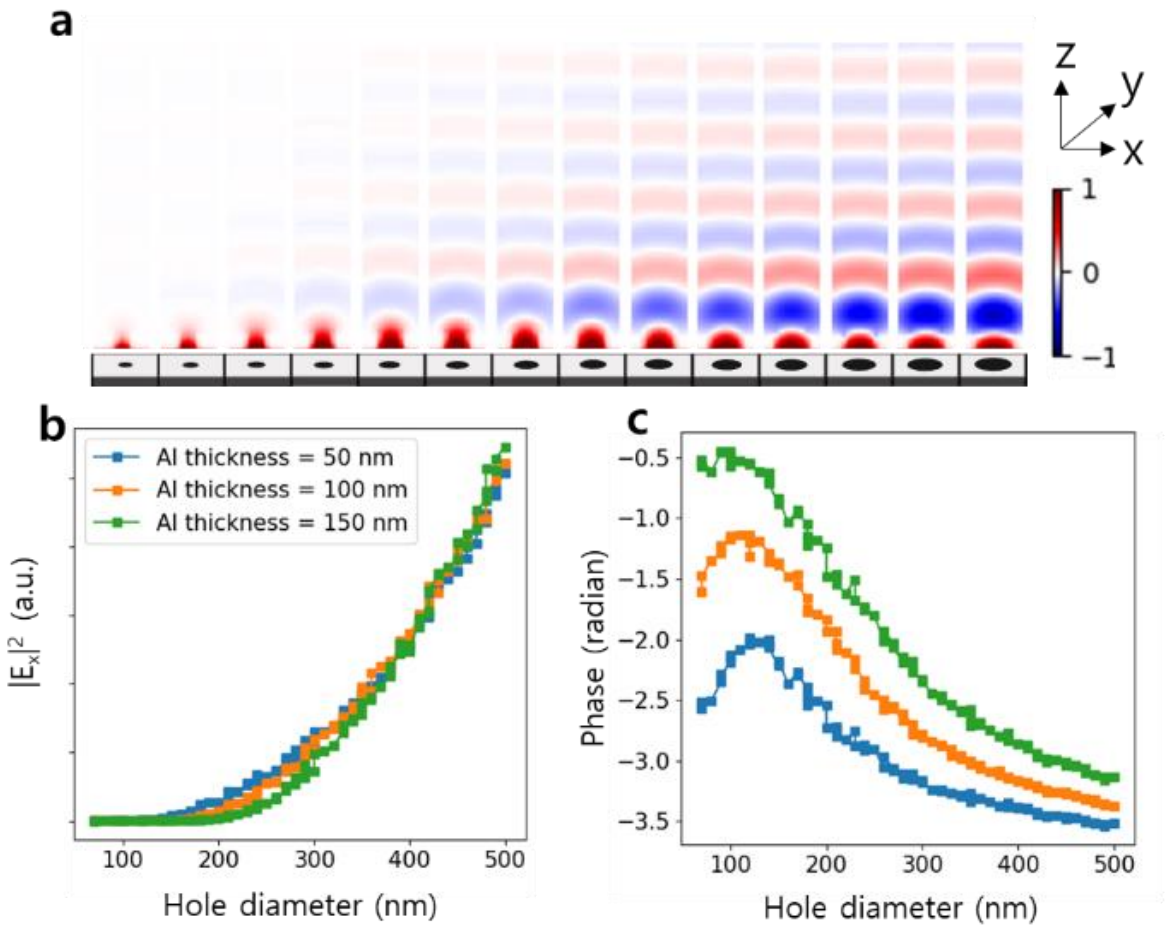

Figure S1 | Light transmission through a single hole. (a) Simulated electric field (E_x) of the light (λ = 650 nm) transmitted through single holes with various diameters (Aluminum layer thickness = 150 nm), normalized by the reference amplitude without the aluminum structure. (b-c) Electric field intensities ($|E_x|^2$) (b), and phases (c) at above $\lambda/2$ from center of the holes with various diameters and aluminum thicknesses.